OMAE-67176

KINEMATICS IN A DIFFRACTED WAVE FIELD: PARTICLE IMAGE VELOCIMETRY (PIV) AND NUMERICAL MODELS

Trygve Kristiansen
Marintek, Trondheim, Norway

Rolf Baarholm
Marintek, Trondheim, Norway

Geir J. Rørtveit
Complex Flow Design, Trondheim, Norway

Ernst W. Hansen
Complex Flow Design, Trondheim, Norway

Carl Trygve Stansberg
Marintek, Trondheim, Norway

ABSTRACT

As the use of CFD in industrial applications increases, so does the need for verification and validation of the theoretical/numerical results. This paper focuses on tools for validation and in particular, on the use of Particle Imaging Velocimetry (PIV) as such a tool. Diffraction of regular waves due to a single, fixed vertical cylinder is investigated. Theoretical results of wave run-up and wave kinematics are compared to measurements from model tests.

Theoretical results are obtained by second order potential theory and by fully non-linear CFD computations. The second order potential theory frequency-domain results are computed by the industry standard code WAMIT, while the fully non-linear time-domain simulations are performed by the commercial CFD code Flow-3D. Measurements are obtained by means of wave probes, PIV and snapshots taken with a high-speed camera. The experiments are made with the model in place as well as without the model, for validation of the incident flow field. For the identification of non-linear effects, the steepness of the waves is varied. The surface elevation is measured by means of the wave probes, while the PIV equipment measures the kinematics. High quality photos taken by the high-speed camera give a detailed overview of the surface elevation for inspection. In addition to focusing on validation tools, the paper also addresses some critical aspects associated with the CFD computations, such as the modeling of boundary conditions.

The work is based partly upon results from the WaveLand JIP, Phase 2.

INTRODUCTION

As the use of CFD in industrial applications increases, so does the need for validation of the theoretical/numerical results. This paper focuses on tools for verification and validation, and in particular on the use of Particle Imaging Velocimetry (PIV) as such a tool. Diffraction due to regular waves on a single, fixed vertical cylinder is investigated.

Wave amplification due to platform legs is an important part of the air gap. In the design and operation of offshore structures, both fixed and floating, wave impact on deck must be taken into consideration. As oil and gas production move to deeper waters, floaters, such as semi-submersibles are becoming increasingly used. The deck height of floaters is limited by weight and stability requirements, and this makes the air gap a substantial cost driver for the structure. The deck's clearance to the free surface may be affected e.g. by failure in ballast systems or a change in production volume. Accurate prediction of the deck clearance to the free surface is therefore of interest.

Diffraction due to regular waves for a single bottom-mounted column is a classical problem, which was solved analytically, assuming linear potential theory, in the early 1950's, see McCamy & Fuchs [1]. However, evidence from experiments that non-linearities may grow significant is found through a variety of studies on single columns, such as in Kriebel [2], Niedzwecki & Duggal [3], Stansberg & Nielsen [4], Stansberg & Braaten [5] and Kristiansen et al. [6]. In [7], diffraction due to a single column as well as the "front" leg of a multi-legged offshore structure was investigated and in [8], air-gap under such structures was investigated.

The use of CFD for computing wave run-up on columns is therefore investigated. Various other nonlinear numerical approaches have also been published, see e.g. Ferrant [9] Malenica et al. [10], ISSC [11] and Ma et al. [12]. Trulsen et al. [13] investigated the problem using a fully non-linear potential code.

PIV, as of today, is regarded as a well established measurement technique for fluid kinematics that is able to bring significant progress to applied fluid mechanics. A significant amount of work has been carried out on developing this tool. A review of some of this work is presented in Stanislas et al. [14]. In most applications, the region investigated is fully covered by one single fluid, but free surface flows have also been analyzed. Free surface flow was investigated by Grue et al. [15], where the kinematics in steep, undisturbed waves were analyzed. In the present work, the kinematics of both moderate and steep diffracted waves is analyzed.

MODEL TESTS

Results from two separate model tests are considered in the present analysis. The test case is a single fixed, vertical, surface piercing circular cylinder in both cases, but in different model scales. One model test measured wave diffraction by means of wave probes, and the other measured wave kinematics by means of PIV. In both model tests, the depth is large enough for the waves to be considered as deep water waves. The particulars of the model tests follow.

Diffraction measurements

In the former model test, four different regular waves, each with three steepnesses were run in the MARINTEK Model Test Tank III in model scale 1:49. In full scale the radius was a=8m, the draft 24m, and water depth 403m. The four regular wave periods were T=7s, 9s, 12s and 15s full scale and the steepnesses H/λ=1/30, 1/16 and 1/10. The model test set-up is illustrated in Figure 1. Wave elevation (diffracted wave) was measured at twelve locations. The wave probes are located radially from the cylinder at 0º, 45º and 90º angles relative to the wave propagation direction, with distance 0.1m, 1.5m, 4.7m and 8.0m from the cylinder wall. In the present analysis, we focus mostly on the two points c_2 and c_4 upwave from the cylinder, but other locations will be considered as well. These model tests will be referred to as the wave diffraction model tests.
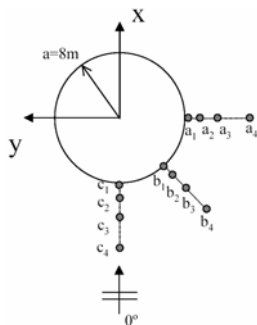

Figure 1. Model test set-up for diffraction model tests.

PIV measurements

Model

The latter model tests were conducted in a glass tank. The model scale was 1:100 (cylinder radius used for scaling). The draft was 45m, and the depth 73m, both values in full scale. Two periods were run with the same three steepnesses as above, but with periods T=8s and 10s. These model tests will be referred to as the PIV model tests. The cylinder draft in the PIV model tests is almost twice that in the diffraction model tests, i.e. 45m vs. 24m. This is considered not to affect the results significantly, at least not by changing the qualitative behavior. This has been investigated at least for wave diffraction in Kristiansen et al. [6], by performing potential theory computations up to second order. Therefore, in the present work, we consider the two model test set-ups to be close to equivalent, at least for wave diffraction and for the kinematics down to a depth of approximately 20m. Prior to the PIV measurements, tests were run with no model present, in order to calibrate the waves.

PIV equipment

The equipment and software used for PIV data acquisition is the *FlowMap Processor* and the *FlowManager Software*, delivered by Dantec. Two CCD-based cameras of type FlowSense M2 10 bit were mounted with a slight angle relative to a line perpendicular to the incoming flow field. With images taken from two angles, it is possible to calculate 3D vector fields. In the present analysis, however, only 2D flow is calculated, since, at least in theory, the flow perpendicular to the incoming wave direction is zero at the positions of c_2 and c_4. The resolution was 1600 x 1186 pixels. Each camera records a series of double exposures. The time between the double exposures is chosen according to different characteristics of the flow, and the exposures are synchronized with a pulsing laser which creates a laser sheet illuminating particles in the fluid. The inverse of the time between the double exposure pairs is denoted as the acquisition frequency, and in the present analysis it was 10Hz. That is, for a wave of period 1s model scale, ten double pairs were needed to capture a full period. In the present model tests, ten pairs were obtained, denoted by image 1-10. An example of an image is shown in Figure 2. The image has been manually masked in order to remove the cylinder and area above the free surface to reduce noise in the analysis. The reflections near the free surface are due to 3D effects of the wave and the model tank glass wall.
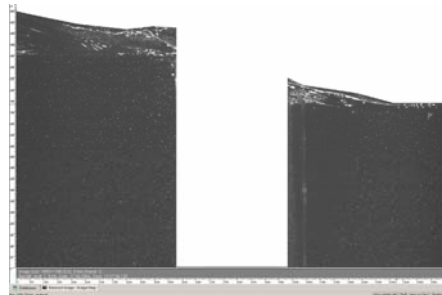

Figure 2. Masked image no. 9. T=10s, H/λ=1/10.

PIV calculations

The kinematics of the diffracted wave field is measured in a vertical plane defined by the laser sheet. The plane goes through the centre of the cylinder and extends approximately one cylinder diameter up-wave and down-wave of the cylinder in the horizontal direction, and approximately from $z=-27m$ up to $z=16m$ in the vertical direction. This is illustrated in Figure 3. Several analysis options of the recorded images are available. These are auto-, cross-, adaptive- and average-correlation. The adaptive-correlation technique is chosen for the present analysis. An interrogation area of 64 x 64 is used. That is, the image, or frame, is divided into squares, each with 64 x 64 pixels, and the particle motion is analyzed within each such square. Discussions of the different techniques may be found in e.g. Stanislas et al. [14]. Figure 3 presents an example of the output from the PIV analysis. Only every fourth velocity vector that is actually calculated is presented here to get a clearer picture of the flow field.
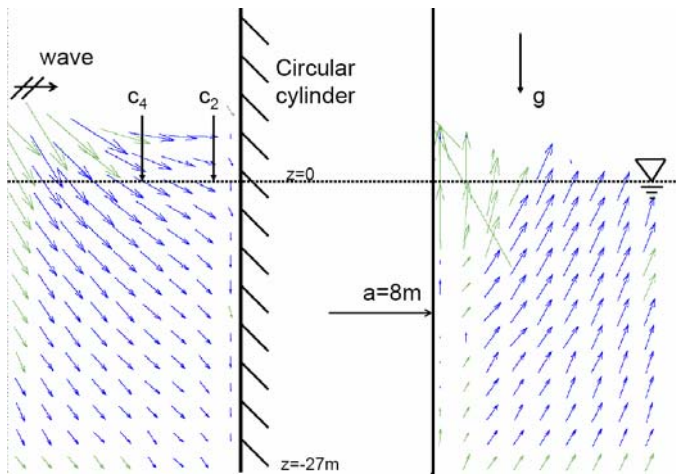

Figure 3. PIV model with velocity vectors. The horizontal dotted line represent the still water level.

In Figure 3, each vector represents the flow velocity at its mid-point. A few spurious vectors are present, e.g. the one behind the cylinder, pointing up to the left. This particular vector is quite easily removed, and does not represent a real problem to the analysis. However, near the free surface, such spurious vectors may be dominating, and do represent a problem. The green color represent substituted vectors, that is, results that have been rejected and substituted by the PIV analysis program based on some validation method, or have been subject to filtering in some way. Typically, this occurs near the boundaries, i.e. near the free surface and the cylinder wall, and the left, bottom and right boundaries of the computational domain. In the present analysis, substituted vectors are treated in the same manner as the other, blue vectors.

An example of high quality photo taken by a high-speed camera (not that used for the PIV-images) is shown in Figure 4. The photo was taken prior to the PIV-tests. Such photos are valuable in investigating the behavior of the fluid qualitatively. No quantitative analysis has been done with regards to this kind of photo in the present analysis.
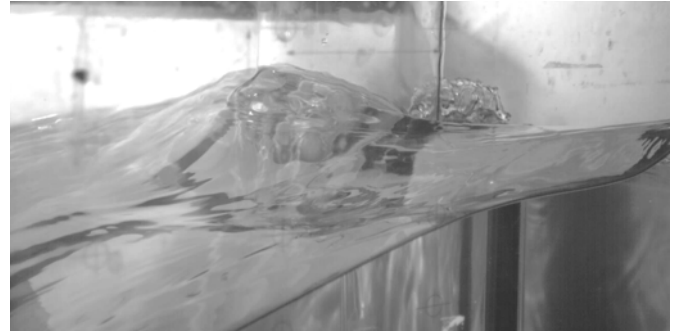

Figure 4. Photo taken by a high-speed camera prior to PIV model tests.

THEORETICAL MODELS

Results from two theoretical models are presented in the present work. One assumes potential theory while the other is based on a Navier Stokes solver (CFD). The models are presented in the following.

Second order potential theory model

Wave diffraction is computed to second order by the standard industrial potential theory code WAMIT (Lee [16]). The WAMIT model used in the present study was also used in Kristiansen et al. [6]. There, convergence of the diffraction RAOs and QTFs was investigated with respect to number of panels on, as well as the extent of the free surface. Satisfactory convergence was reached for both the linear and second order terms. The number of panels on the body was $N_B=2640$, and on the free surface $N_F=16000$, which was the highest resolution that was used in the convergence tests. The number of panels refers to the full domain, whereas symmetry allowed for only one quarter of the domain to actually be modeled. The partition radius was 30m. The resolution of the free surface was found to be the main contributor to convergence, while a large partition radius was not. This is consistent with the findings of Birknes [17]. The WAMIT model with a low resolution for better visualization is shown in Figure 5.
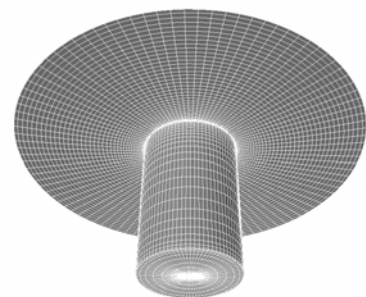

Figure 5. WAMIT model of the circular cylinder with free surface mesh. Here, $N_B=2640$ and $N_F=2800$ (total surface).

Potential theory assumes that the fluid has zero viscosity. The validity of the results therefore depends on the amount of viscous effects in the particular flow. It is believed, however, that viscous effects may be significant at least in some parts in the vicinity of the structure.

CFD model

Numerical simulations have been performed using the commercial CFD code Flow-3D, which applies the finite volume method to solve the three-dimensional Reynolds-Averaged Navier-Stokes (RANS) equations. The prediction of the free surface in the program is based on the volume tracking method VOF (Volume Of Fluid), see Hirt & Nichols [18]. This method is developed to simulate highly nonlinear effects such as breaking waves at the interface, although, no such breaking effects have been observed in the current analysis. The VOF method in Flow-3D has been improved beyond the original VOF method, see Barkhudarov [19]. For wave propagation problems, special boundary treatments have been devised in Flow-3D, see Hirt [20]. The outflow boundary condition is set in such a way as to allow their continuation through the boundary with a minimum of reflection. Orlanski [21], describes an early and useful example of this type of treatment, sometime called a radiation boundary condition, or Sommerfeld condition.

A numerical wave tank has been modeled, as shown in Figure 6. A wave maker located at the left boundary generates waves going from left to right. The wave maker imposes fluid velocity according to linear theory. Linear extrapolation to the free surface is implemented. The waves are gravity driven. The still water height is 70m (z-direction) while the total height of the domain is 100m, the width is 80m (y-direction), and the length is 156m (x-direction) which is one linear wave-length of the 10s wave. The VoF method requires discretization of the full domain, including the volume above the free surface. In general, each grid cell is 1.0m in all three directions. Exceptions are near the side walls, where 2.0m is used, and near the bottom, where the cell height goes up to 12m. A total of approximately half a million grid cells is used (N_x=158, N_y=62 and N_z=52). The fluid is water given by its density. Turbulence is modeled by an RNG model.
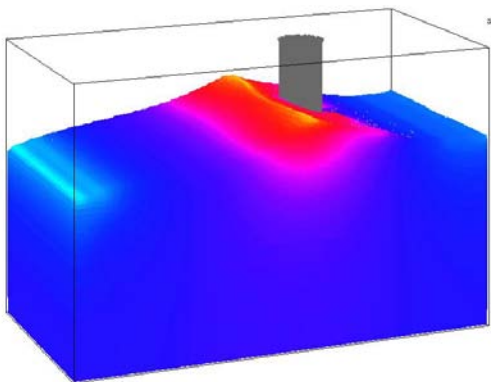

Figure 6. CFD computational domain. Wavemaker located at left boundary. T=10s, H/λ=1/10.

As mentioned, the outlet is implemented as a radiation boundary. Some problems, that are perhaps associated with this, however, arose in the initial phase of the modeling. The total fluid volume was increased by approximately 4% at the instant the wave reached the downstream boundary. However, since the wave front (and energy) travels with the group velocity, which for deep water is half the phase velocity, this occurs after two wave periods for a tank of one wave length. The second wave in the wave train may therefore be used for the present analysis. Long time series have been achieved in previous works, such as in Ferrant et al. [22], Ma et al. [12] and Ohl et al. [23]-[24]. More work is needed in order to improve the current model if longer time series are desired. Time series of the wave with the three steepnesses measured 40m upstream from the cylinder centre is shown in Figure 7. In Figure 8, a snapshot of the velocity field around the cylinder is shown.
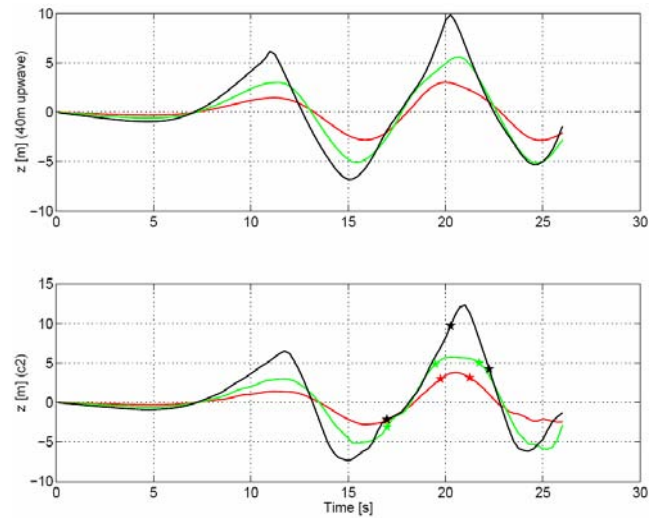

Figure 7. Wave elevation 40m upwave from cylinder centre and at c_2 in CFD computations. T=10s, H/λ=1/30, 1/16 and 1/10.
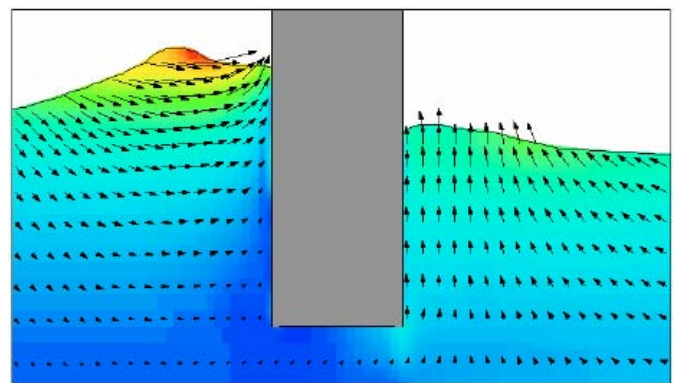

Figure 8. Snapshot of velocity field computed by CFD.

RESULTS

Validation of the CFD results is done separately for free surface elevation and fluid particle kinematics. First, comparisons to the diffraction model test results as well as WAMIT computations are made to validate the free surface elevation. Then the fluid kinematics are compared to the PIV model test results.
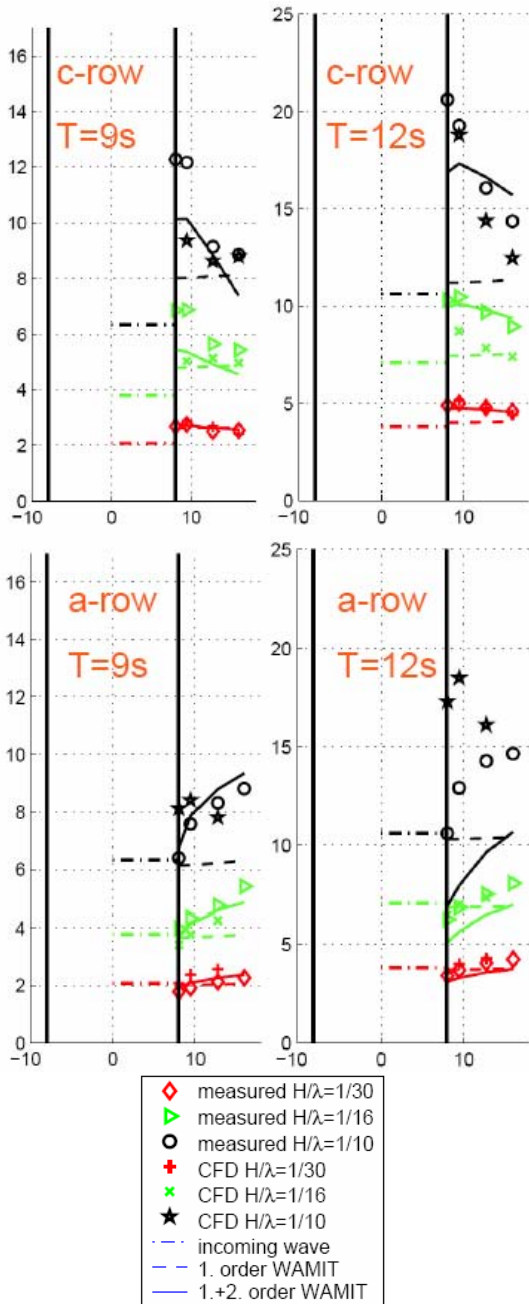

Figure 9. Measured vs. calculated run-up. T=9s and 12s.

CFD vs diffraction measurements

Validation of the wave diffraction is made for two wave periods, T=9s and 12s, and at six locations, points c_2, c_3 and c_4 which are located directly upwave from the column, and points

a_1, a_2 and a_3 which are located 90 degrees out from the cylinder relative to the wave direction, as shown in Figure 1. The results are shown in Figure 9. Upwave (c-row), both theoretical models in general under predict, although in some cases, both show quite good comparison to the model test results. The CFD seems to capture the jet-like run-up on c_2 for the longest period, but not for the short period. The potential theory results do not capture this jet for any of the periods, but this is as expected. To the side of the cylinder (a-row), the CFD in general over-predict, while the potential theory under-predicts. An exception is the medium steepness, where measurements and CFD corresponds well. For the largest steepness, however, the CFD results highly over predict to the side of the cylinder. One possible cause may be unwanted reflections from the side walls. Except for the mentioned discrepancies, the qualitative behavior seems to be quite reasonably captured.

CFD vs PIV measurements

Velocity profiles at the two locations c_2 and c_4 for the horizontal and vertical velocity components are investigated. To keep the number of figures at a reasonable level, only two locations are included, and three time instants are considered. The time instants represent three phases of the wave evolution. The first time instant is just after the crest has passed, the second just before it reaches still water level (uprising), and the third just before the crest passes. These are denoted by PIV images no. 01, 06 and 09, as shown in Figure 11. Two instants near the crest are chosen as that is where the highest velocities occur, and events of high wave elevation combined with high velocities are of interest with respect to e.g. slamming beneath platform decks. It is therefore of particular interest to validate the theoretical/numerical results here.

Synchronization

CFD results were stored with a time increment of 0.25s full scale, so a fairly good, although not perfect, synchronization between the measured and theoretical results is possible. The synchronization is based on the wave time-series shown in Figure 10. The markers indicate the chosen time instants used in the comparisons. In general, the time instants used for the highest steepness are somewhat later than for the lower steepnesses. This is explained by the non-linear speed-up of the phase speed. To second order, the phase velocity is in deep water given by

$$c_p = \frac{g}{2\pi}\left(1+\left(k_0 A\right)^2\right)T , \qquad (1)$$

where g is the acceleration of gravity, k is the linear wave number, and A is the linear amplitude. Thus, the steepest wave travels about 8% faster than the lowest wave. Therefore, the wave phase at the instant the photo is taken depends on the steepness. The waves in the PIV model wave tank travel about two wave-lengths before it reaches the column, whereas in the numerical wave tank, they travel approximately one wave-length, and the PIV image capturing is initiated exactly 8s (model scale) after the wave maker starts for all three waves. Further, the numerical wave is not entirely developed, whereas the model test wave is expected to be developed. The three

Copyright © 2005 by ASME

subjects addressed, a time increment of 0.25s in the CFD results, non-linear phase speed, and wave development all gives rise to some uncertainties in the synchronization. In our experience, there is an uncertainty of +/- 0.25s, but within that uncertainty, the synchronization is quite good.
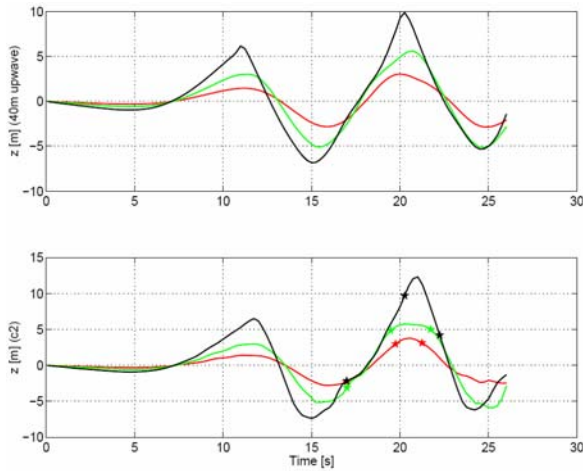
Figure 10. Undisturbed wave (CFD) 40m upwave from cylinder centre (top), and diffracted wave at c_2 (bottom). T=10s. H/λ=1/30, 1/16 and 1/10. Symbols represents PIV image (from left to right) 06, 09 and 01

Calibrated wave

In Figure 12 and Figure 13, kinematics for the undisturbed, calibrated wave for the medium wave steepness (H/λ=1/16) is shown. As far as the calibrated PIV waves go, only the medium steepness was recorded. The CFD results are taken 40m upwave of the cylinder centre, and is considered to be unaffected by the structure. Except for a slightly larger horizontal velocity component in the CFD computations

compared to the PIV measurements just below the surface, the agreement is good for the undisturbed wave. The linear velocity profile is also included in the figures. The synchronization is based on an assumed zero-crossing point of the underlying linear wave at found from inspection of Figure 10 (no Fourier analysis was possible due to short time series). Any large discrepancy from the linear velocity profile far below z=0 should be considered to be due to synchronization problems. This seems to have been achieved quite successfully, and the non-linearities close to the free surface are clearly observed. No stretching to the free surface has been performed.

Diffracted wave

In Figure 14 and Figure 15, diffracted kinematics for the points c_2 and c_4 (with the cylinder in place) is shown. It seems in general that the kinematics as computed by CFD agrees reasonably well with those measured by PIV. A possible trend may be that the horizontal velocities are slightly over predicted, while the vertical velocities are slightly under predicted by the CFD computations.

The trend with increasing velocities with increasing steepness is clearly non-linear, as expected. This, of course, is most easily observed near the surface.

For PIV image 09, a discrepancy from the expected is observed near the surface (for 5m<z<10m) in the horizontal component both at point c_2 and c_4. Inspection of results in the vicinity of the two points, however, reveals much smoother behavior near the surface. Reflections on the free surface may be a possible explanation, as seen in Figure 11. In the vertical direction, the measurements agree well with the computations also near the surface, though, so the distortions are not yet fully understood.
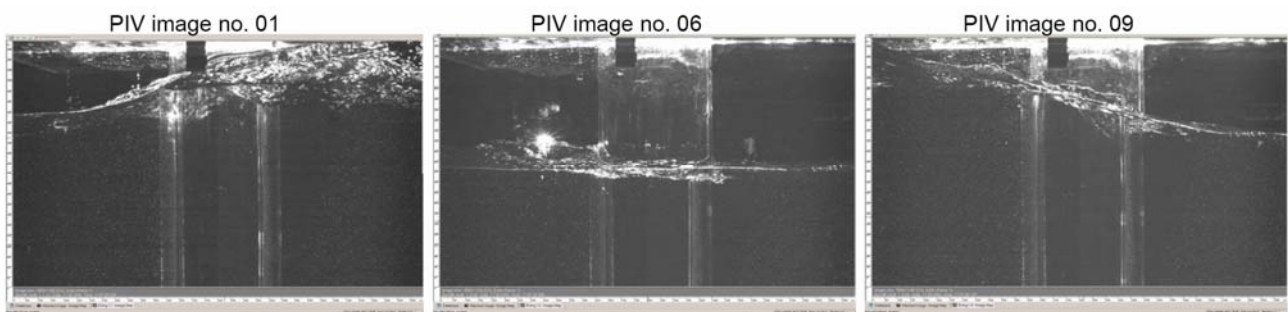
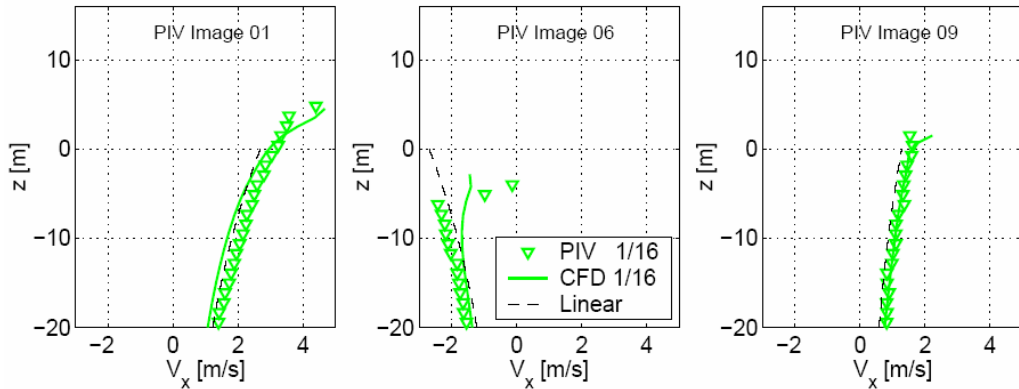**Figure 11. PIV images as taken by the FlowSense M2 camera. T=10s, H/λ=1/10. Image is taken from a slight angle.**

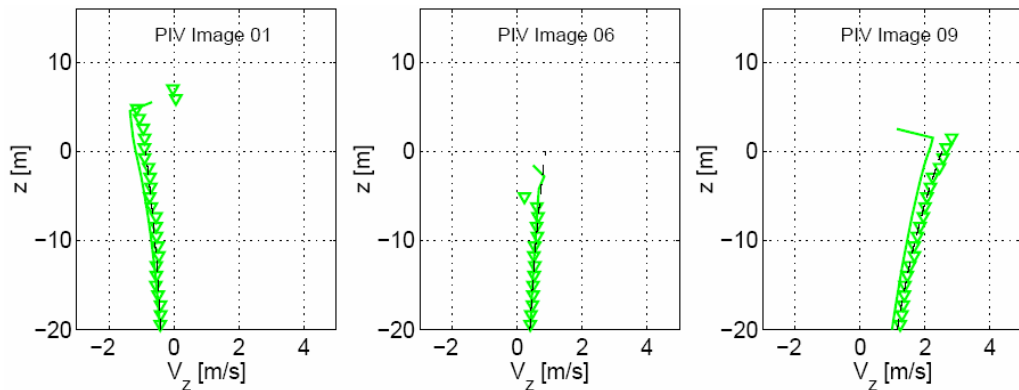**Figure 12. Horizontal wave component in undisturbed, calibrated wave. T=10s, H/λ=1/16.**

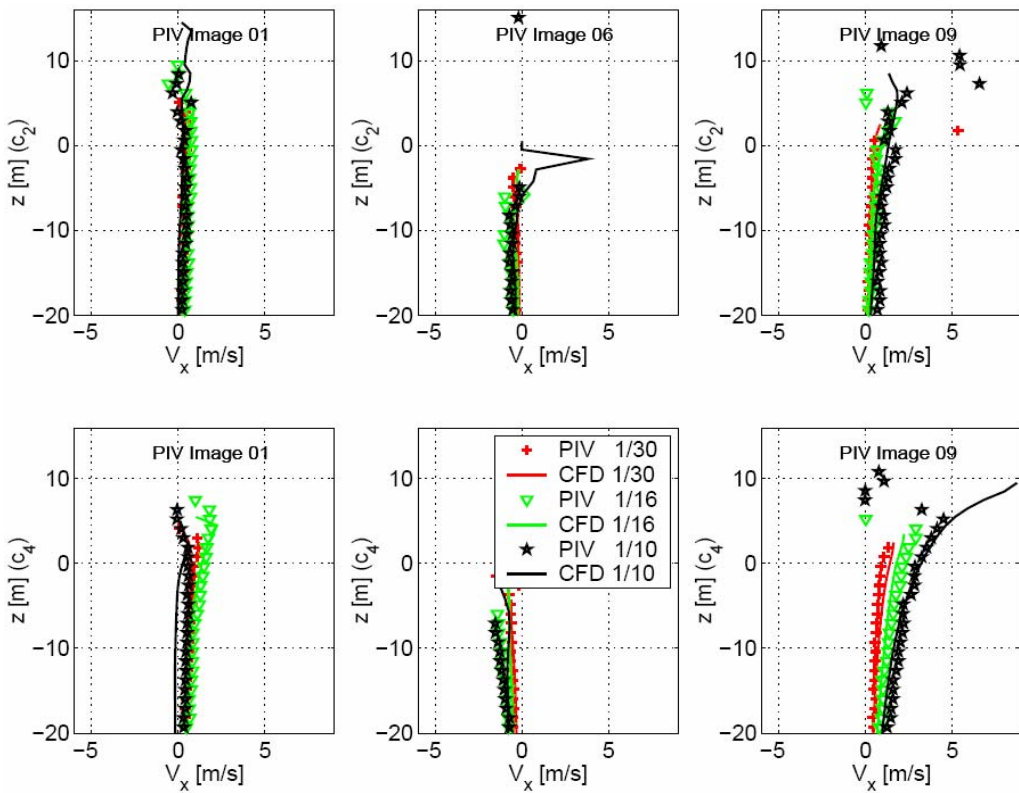**Figure 13. Vertical wave component in undisturbed, calibrated wave. T=10s, H/λ=1/16.**

Figure 14. Comparisons of horizontal wave component as measured by PIV (symbols) and computed by CFD (curves). T=10s. Three steepnesses: H/λ=1/30, 1/16 and 1/10.

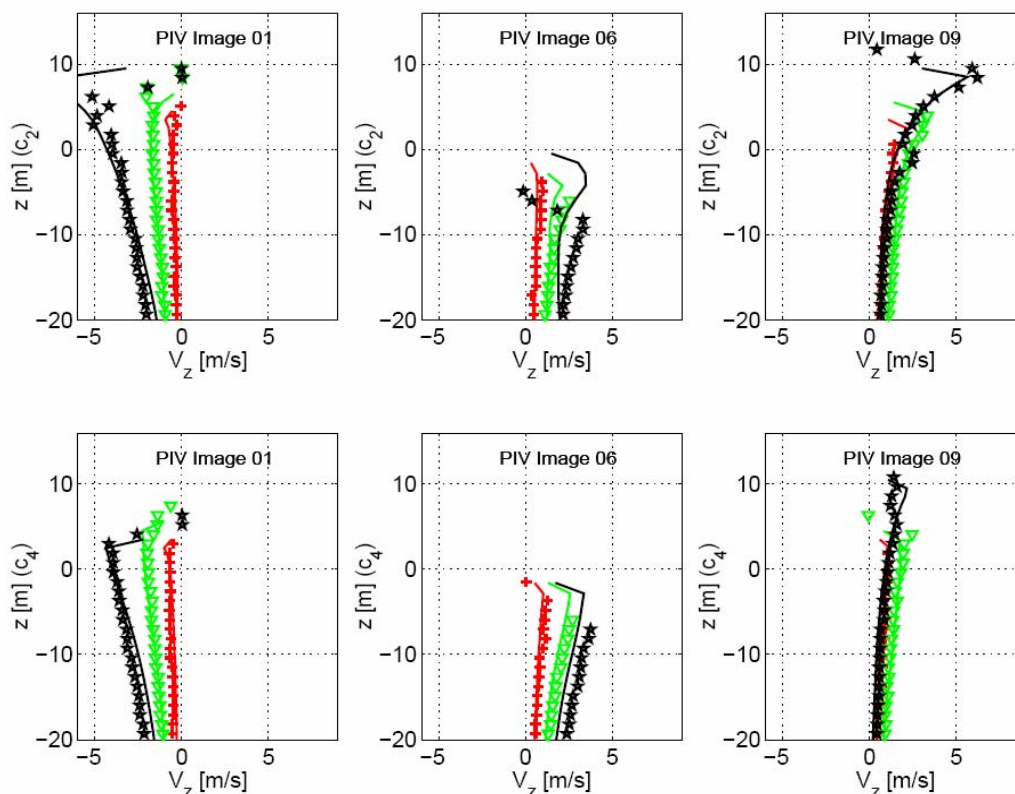**Figure 15. Comparisons of vertical wave component as measured by PIV (symbols) and computed by CFD (curves). T=10s. Three steepnesses: H/λ=1/30, 1/16 and 1/10. Legend as in**

CONCLUSIONS

CFD computations of incoming regular waves on a single, circular, fixed vertical cylinder have been validated against model test results. The main focus was on using Particle Imaging Velocimetry (PIV) as a tool for validation of the computed wave kinematics. Free surface diffraction was also validated against model tests as well as compared to potential theory results.

Theoretical results were obtained by second order potential theory and by fully non-linear CFD computations. The second order potential theory results were computed by the industry standard code WAMIT, while the fully non-linear simulations were performed by the commercial CFD code Flow-3D.

Measurements were obtained through two separate sets of model tests. One of the model tests obtained measurements of the kinematics by means of PIV, in model scale 1:100, and the other model tests obtained diffraction measurements by means of wave probes, in model scale 1:49. Experiments were carried out with, as well as without, the model in place, such that validation of the incident flow field could be done. For the identification of non-linear effects, the steepness of the waves was varied. Waves with three steepnesses were run, with H/λ=1/30, 1/16 and 1/10 in both sets of model tests.

Some scatter in the PIV results was seen near the free surface. This was only the case for the horizontal velocity component, and perhaps caused by undesired reflections. In general, however, the PIV results seemed to be of reasonably good quality.

The qualitative behavior of the CFD results were captured reasonably well, although few discrepancies were observed between measured and computed values. As far as the undisturbed waves go, the kinematics were reconstructed quite well by the CFD computations. Also in the diffracted field (with the model present), the kinematics were reasonably reconstructed.

In addition to focusing on validation tools, the paper also addressed some critical aspects associated with the CFD computations, such as the modeling of boundary conditions. The total volume of the fluid rose after the waves reached the outflow boundary, and the simulations were therefore only run up to this time. Some more work is needed for longer time-series, although the results were considered adequate for the present work.

REFERENCES

[1] McCamy, R. and Fuchs, R. (1954), "Wave Forces on Piles: A Diffraction Theory", *Tech. Memo No. 69, Beach Erosion Board, U.S. Army Corps of Engineers,* Washington D.C, USA.

[2] Kriebel, D. (1992), "Nonlinear Wave Interaction with a Vertical Circular Cylinder. Part II: Wave Run-up", *Ocean Engineering, Vol. 19,* pp. 75-99.

[3] Niedzwecki, J.N. and Duggal, A.S. (1992), "Wave Run-up and Forces on Cylinders in Regular and Random Waves", *J. Waterways, Port, Coastal, and Coastal Engineering,* ASCE, Vol. 118, pp. 615-634.

[4] Stansberg, C.T. and Nielsen, F.G. (2001), "Nonlinear Wave-Structure Interaction on Floating Production Systems", *Proc., Vol. IV, the 11th ISOPE Conference*, Stavanger, Norway, pp. 363-372.

[5] Stansberg, C.T. and Braaten, H. (2002), "Nonlinear wave disturbance around a vertical circular column", *Proc. Paper No. OMAE2002-28620, 21st OMAE Conference*, Oslo, Norway 2002.

[6] Kristiansen, T., Baarholm, R. and Stansberg, C. T. (2004), "Validation of second-order analysis in predicting diffracted wave elevation around a vertical circular cylinder", *Proc., Vol I,, 14th ISOPE Conf.*, Toulon, France, pp 342-349.

[7] Stansberg, C. T. and Kristiansen, T. (2005), "Non-linear scattering of steep waves around vertical columns.", *Appl. Ocean Res.* (in review).

[8] Nielsen, F.G. (2003), "Comparative study on airgap under floating platforms and run-up along platform columns.", *J. Marine Struct,* Vol 16, pp 97-134.

[9] Ferrant, P. (1999), "Fully Nonlinear Diffraction of Regular Waves by a Multicolumn Structure", *Proc., Vol. III, 9th ISOPE Conf.*, Brest, France.

[10] Malenica, S. and Eatock Taylor, R. (1999). "Second-order water wave diffraction by an array of vertical cynders", *J. Fluid Mech.,* Vol. 390, pp 349-373.

[11] ISSC (2000), Report from the 14th International Ship and Offshore Structures Congress, Technical Committee I.2: Loads, Nagasaki, Japan.

[12] Ma Q. W., Wu G.X. and Eatock Taylor R. (2001). "Finite element simulations of fully non-linear interaction between vertical cylinders and steep waves. Part 2: Numerical results and validation", *Int. J. Num. Met. Fluids,* Vol. 36, pp 287-308.

[13] Trulsen, K. and Teigen, P. (2002), "Wave scattering around a vertical cylinder: Fully nonlinear potential flow calculations compared with low order perturbation results and experiments", *Proc., Paper No. OMAE02/OFT-28173, OMAE 2002 Conf.*, Oslo, Norway.

[14] Stanislas, M., Kompenhans, J., Westerweel J. (Eds.) (2000), "Particle Image Velocimetry. Progress towards Industrial Applications.", *Fluid Mechanics and its Applications*, Kluwer Academic Publishers

[15] Grue, J., Clamond, D., Huseby, M. and Jensen, A. (2004), "Kinematics of extreme waves in deep water.", *Appl. Ocean Res.* Vol 25, pp 355-366.

[16] Lee C.-H. (1995), "WAMIT Theory Manual", *Report No. 92-2, Dept. of Ocean Engineering*, Massachusetts Institute of Technology (MIT), Cambridge, Mass., USA.

[17] Birknes, J. (2001), "A convergence Study of Second-Order Wave Elevation on Four Cylinders", *Proc., Vol. III, the 11th ISOPE Conf.*, Stavanger, Norway.

[18] Hirt, C.W. and Nichols, B.D. (1981), "Volume of Fluid (VOF) Method for the Dynamics of Free Boundaries.", *J Comp. Phys.,* Vol 39, pp 201.

[19] Barkhudarov M.B. (2003) "Semi-Lagrangian VOF Advection Method in Flow-3D,", *Flow Science Inc., Technical Note, FSI-03-TN63.*

[20] Hirt, C. W. (1999), "Addition of Wave Transmitting Boundary Conditions to the Flow-3D Program.", *Flow Science Inc., Technical Note, FSI-99-TN49.*

[21] Orlanski, I. (1976), "A Simple Boundary Condition for Unbounded Hyperbolic Flows", *J. Comp. Phys.,* Vol 21, 251-269.

[22] Ferrant, P., Touzé, D. L. and Pelletier, K. (2003), "Non-linear time-domain models for irregular wave diffraction about offshore structures", *Int. J. for Numer. Meth. Fluids*, Vol 42.

[23] Ohl, C. O. G., Eatock Taylor, R., Taylor, P. H., Borthwick, A. G. L., (2001), "Water wave diffraction by a cylinder array. Part I. Regular waves", *J. Fluid Mech.,* Vol 442, pp 1-32.

[24] Ohl, C. O. G., Eatock Taylor, R., Taylor, P. H., Borthwick, A. G. L., (2001), "Water wave diffraction by a cylinder array. Part II. Irregular waves", *J. Fluid Mech.,* Vol 442, pp 33-66.